Journal of Power Sources 242 (2013) 50–56

Contents lists available at SciVerse ScienceDirect

Journal of Power Sources

journal homepage: www.elsevier.com/locate/jpowsour

Synthesis, physical–chemical characterization and electrochemical performance of $GdBaCo_{2-x}Ni_xO_{5+\delta}$ ($x = 0$–0.8) as cathode materials for IT-SOFC application

Y. Hu [a], C. Bogicevic [a], Y. Bouffanais [a], M. Giot [a,b], O. Hernandez [c], G. Dezanneau [a,*]

[a] Laboratoire SPMS, Ecole Centrale Paris (UMR CNRS 8580), Grande voie des vignes, 92295 Chatenay-Malabry Cedex, France
[b] Manufacture Française des Pneumatiques Michelin, Centre de technologies, 63040 Clermont-Ferrand, France
[c] Institut des Sciences Chimiques de Rennes (équipe Chimie du Solide et Matériaux), UMR 6226 CNRS-Université de Rennes 1, Bât. 10B, Campus de Beaulieu, F-35042 Rennes, France

HIGHLIGHTS

- Ni-doped $GdBaCo_2O_{5+d}$ cathode materials have been studied.
- Ni-doped $GdBaCo_2O_{5+d}$ compounds possess the same structure as pure GBCO.
- Ni-doping leads to a same oxygen content but to a lower transition temperature.
- The thermal expansion coefficient slightly diminishes with Ni-doping.
- Electrochemical performance slightly increase with Ni-doping.

ARTICLE INFO

Article history:
Received 11 October 2012
Received in revised form
14 March 2013
Accepted 9 May 2013
Available online 21 May 2013

Keywords:
IT-SOFC
Cathode
$GdBaCo_{2-x}Ni_xO_{5+\delta}$
Oxygen content
Phase transition
Impedance spectroscopy

ABSTRACT

$GdBaCo_{2-x}Ni_xO_{5+\delta}$ ($x = 0$–0.8) cathode materials have been synthesized by a citrate-gel modified chemical route, by which we have achieved a high level of substitution up to $x = 0.8$. Oxygen stoichiometry at room temperature has been determined by iodometry and the structural evolution as a function of Ni content has been extracted from XRD patterns analysis. All compounds are orthorhombic at room temperature and a DSC analysis reveals that the high-temperature orthorhombic-to-tetragonal phase transition is observed at lower temperature as Ni substitution increases. Three compositions, with $x = 0$, 0.3 and 0.6, were then chosen for further characterization: high-temperature XRD has been performed confirming the abovementioned structural evolution with temperature and allowing to determine that Ni doping diminishes slightly the thermal expansion coefficient. According to 4-probe measurements, we show that these compounds present a high electronic conductivity, suitable for cathode materials. Finally, electrochemical characterization has been performed by AC impedance spectroscopy with symmetric cells using composite electrode showing an improvement of performance at intermediate substitution levels.

1. Introduction

The double perovskite compound $GdBaCo_2O_{5+\delta}$ (GBCO) was presented years ago as a promising cathode material for solid oxide fuel cells (SOFCs) [1–3]. Such an assumption was based on the high conductivity of this GBCO material combined with the observation of very fast oxygen exchange and diffusion coefficients. This was later on confirmed by Tarancón et al. [4], who investigated intrinsic oxygen transport properties of $GdBaCo_2O_{5+\delta}$ using ion exchange depth profile/secondary ion mass spectrometry method and proved that it exhibits suitable tracer diffusion and surface exchange coefficients with low activation energies in comparison with other mixed ion-electron conducting cobaltites such as $La_{1-x}Sr_xCoO_{3-d}$ (LSC) and $La_{1-x}Sr_xCo_{1-y}Fe_yO_{3-\delta}$ (LSCF). Electrochemical characterization using symmetric cells with $La_{1-x}Sr_xGa_{1-y}Mg_yO_{3-\delta}$ (LSGM) and $Ce_{1-x}Gd_xO_{2-\delta}$ (CGO) electrolytes allowed obtaining an area specific resistance (ASR) of 0.25 Ω cm^{-2} at $T \sim 650$ °C, and the fuel cells test carried out with the configuration GBCO/LSGM/CGO/Ni-CGO using air and H_2 as oxidant and fuel, respectively,

* Corresponding author.
E-mail address: guilhem.dezanneau@ecp.fr (G. Dezanneau).

0378-7753/$ – see front matter © 2013 Elsevier B.V. All rights reserved.
http://dx.doi.org/10.1016/j.jpowsour.2013.05.043

demonstrated a maximum power density of 180 mW cm^{-2} at 800 °C [5]. The chemical diffusion and surface exchange coefficients were also investigated using electrical conductivity relaxation [6]. Generally, excellent performance has been shown for oxygen transport coefficients, polarisation resistance and electronic conductivity for $GdBaCo_2O_{5+\delta}$ in the temperature range of interest [6–8], allowing to consider this material as a good cathode candidate for intermediate or even low-temperature SOFC application.

Nevertheless, similarly to other $LnBaCo_2O_{5+\delta}$ (Ln = lanthanides) compounds with comparatively large thermal expansion coefficient (TEC), the TEC obtained for $GdBaCo_2O_{5+\delta}$, e.g. 16.0–20.0 × 10^{-6} K^{-1} [7,9,10] is significantly higher than those of typical electrolytes such as Yttria-stabilised Zirconia (YSZ), CGO and LSGM, giving rise to component mismatch during the cell fabrication and the operational thermal cycling. In order to adjust the thermal expansion and to optimize the electrochemical performance, one school of thoughts is the B-site substitution for Co by other transition metals such as Ni and Fe, by which great improvements have been achieved in the LSC type perovskite materials, such as lower thermal expansion, better chemical stability or enhanced electrode performance [11–16]. However, yet only a few attentions have been paid on the double layered perovskite materials, e.g. $GdBaCo_2O_{5+\delta}$ [17–19], moreover with only limited substitution level.

The objective of this study is to explore new cathode materials based on $GdBaCo_2O_{5+\delta}$ by performing Ni substitution on B-site aiming at altering its physical-chemical properties. We paid special attention to the structural evolution with substitution, oxygen nonstoichiometry and high-temperature phase transition. Furthermore, three compositions with different Ni substitution levels (x = 0, 0.3, 0.6) were selected for thorough characterization such as electrical conductivity, thermal expansion, and electrochemical performance.

2. Experimental details

An acrylic acid polymerization method was used to fabricate the pristine $GdBaCo_2O_{5+\delta}$ and Ni-substituted $GdBaCo_{2-x}Ni_xO_{5+\delta}$ (with x = 0.1–0.8 every 0.1). Nitrate precursors $Gd(NO_3)_3{\cdot}6H_2O$ (99.9%-Gd, STREM), $Ba(NO_3)_2$ (99%, Alfa Aesar), $Co(NO_3)_2{\cdot}6H_2O$ (99%, STREM), $Ni(NO_3)_2{\cdot}6H_2O$ (99.9%-Ni, STREM) were completely dissolved in de-ionized water in stoichiometric ratio with magnetic stirring, then citric acid monohydrate ($C_6H_8O_7{\cdot}H_2O$, 99.5–100%, MERCK) was added as a chelating agent with the proportion n(citric acid):n(total positive charges of metallic cations in solution) = 1:2, resulting in a clear transparent solution. The pH of the solution was adjusted to 6 at 70 °C by ammonia addition. The solution was heated till boiling, afterwards acrylic acid (99%, SIGMA–ALDRICH) (1/10 of the original volume of solution) and N,N′-methylene-bis-acrylamide (98%, SIGMA) with a concentration of 5.6 g/L were added with continuous heating. Then, several droplets of hydrogen peroxide were added as a polymerization initiator, until the two monomers reacted together forming an organic 3D tangled network, a transparent gel. The gel was further dried in a microwave oven for 30 min, and then grinded and pre-heated at 500 °C for 1.5 h. The obtained precursor was well grinded and finally heat-treated at 1050 °C for 5 h, resulting in the desired $GdBaCo_{2-x}Ni_xO_{5+\delta}$ (x =0, 0.1, 0.2, …, 0.8) compounds. Finally, after a last manual grinding, an air-annealing process was carried out at 900 °C for 3 h for all the as-synthesized powders with a slow cooling rate of 100 C/h in order to ensure an oxygen content close to that of thermodynamic equilibrium.

The as-synthesized powders were characterized by X-ray powder diffraction (XRD, Rigaku D/max-2550/pc, Cu Kα radiation). Refinements of XRD patterns were performed with the Fullprof suite program [20,21] to extract the evolution of crystal structure as a function of Ni substitution. The powder and electrode morphology was investigated using scanning electron microscopy (SEM Hitachi S-4700). Oxygen content was identified according to the different methods fully described in previous references [22,23]. Iodometric titration method was applied for all Ni-substituted compounds, while thermogravimetric hydrogen reduction (TG/H_2 reduction) method was performed (SETARAM 92-1750) for $GdBaCo_2O_{5+\delta}$, $GdBaCo_{1.7}Ni_{0.3}O_{5+\delta}$ and $GdBaCo_{1.4}Ni_{0.6}O_{5+\delta}$, abbreviated to GBCO, GBN03 and GBCN06, respectively. In TG/H_2 measurement, the powder samples (*c.a.* 100 mg) were heated up to 950 °C at a rate of 2 °C/min in a mixed 5% H_2–95% Ar gas flow (5 L/h), followed by an isothermal period of 5 h. All the measurements have been carried out with correction of blank experiments with alumina powder to take into account buoyancy effects.

DSC has been used to prove the existence of the high-temperature phase transition and to determine precisely this transition temperature. These measurements were carried out using a SETARAM TG/DSC, Model 92-1750 instrument, in static air condition following a heating/cooling rate of 5 °C/min till/from 700 °C. High-temperature XRD (25–700 °C) were carried out in air condition, on a rotating anode diffractometer (Rigaku Rotaflex RA-HF18) using Cu $K_{\alpha 1,2}$ radiation.

Electrical conductivity was measured on the three GBCO, GBCN03 and GBCN06 materials. Rectangular bar samples were formed by uniaxial pressing followed by cold isostatic pressing, and successively sintered at 1200 °C for 12 h, obtaining densities close to 90%. Au paste and Au wires were used to form four points' contacts on the bar samples which were mounted on an ionic-systems sample holder. AC conductivity was measured at 1 kHz using a digital lock-in amplifier (SR850, Stanford research system) under an air flux of 5 L/h from room temperature to 800 °C.

Electrochemical properties were characterized by electrochemical impedance spectroscopy (EIS) on symmetric cells with composite electrodes, using CGO as electrolytes. The CGO substrates were prepared from a commercial powder (CGO 90/10SY UHSA, ANAN), by cold isostatic pressing at 750 MPa and sintering at 1450 °C for 12 h, achieving high density (96–97% of theoretical density). Composite electrodes were prepared by the mixture of 50 wt.% CGO – 50 wt.% $GdBaCo_{2-x}Ni_xO_{5+\delta}$ dispersed in ethanol with an organic dispersant (Tween20, Sigma–ALDRICH), followed by a stirring of several days in order to obtain well dispersed suspension ink. The ink was then symmetrically deposited on the two surfaces of CGO electrolyte substrates by airbrush spraying then sintered at 1100 °C for 3 h. To ensure good electric contacts, gold paste (METALOR, GOLD PASTE M-0034) was coated onto the electrodes to form an Au layer serving as current collector. AC impedance spectroscopy was performed at open circuit voltage (OCV) using a Solartron 1260 frequency response analyzer, with applied amplitude of 50 mV over the frequency range from 0.01 Hz to 10 MHz. The temperature dependence measurements were conducted over the 300–800 °C temperature range in air. Zview 2 electrochemical impedance software (Scribner Associates Inc.) was used for data analysis.

3. Results and discussion

3.1 Phase characterization and structural evolution

Fig. 1 shows the room temperature XRD patterns of $GdBaCo_{2-x}Ni_xO_{5+\delta}$ compounds synthesized from the polymerization route followed by a heat-treatment at 1050 °C for 5 h in air. With Ni substitution, pure phase could be guaranteed until the substitution proportion x = 0.8, maintaining a structure similar to the pristine GBCO indexed in the orthorhombic *Pmmm* space group. This reveals a higher level of solubility compared to previously reported studies

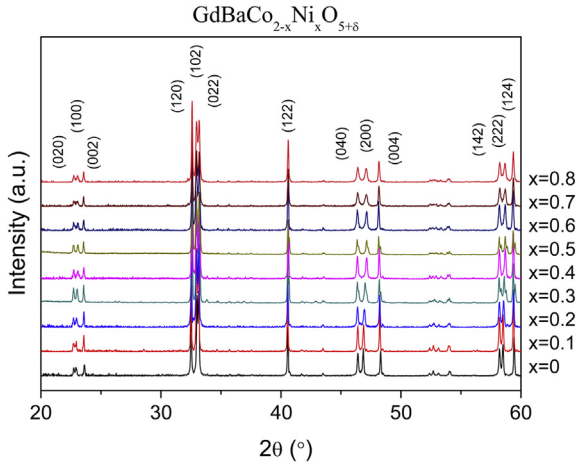

Fig. 1. XRD patterns of $GdBaCo_{2-x}Ni_xO_{5+\delta}$, $x = 0$–0.8 indexed to orthorhombic structure with *Pmmm* symmetry.

[19,24]. This increased solubility of Ni is certainly favored by the fabrication route which allows obtaining a highly homogeneous precursor. The increase of Ni substitution level gives rise to the shift of peak positions as well as an increase to the (040) and (200) peak splitting according to the XRD pattern. This indicates that the Ni substitution for Co would enhance the orthorhombic distortion, in agreement with the systematic increase in "orthorhombicity" by Ni substitution in GBCO observed by Bharathi et al. [24].

The evolution of cell parameters has been extracted from Rietveld refinement on XRD data, according to the structure model in reference [20,21,25], as exemplified in Fig. 2. The evolution of cell parameters and of the unit cell volume ($a_p \times a_p \times a_p$) with Ni substitution are shown in Fig. 3. For $x \leq 0.4$, with increasing Ni, a decrease of the *a*-lattice parameter is observed, whereas both *b* and *c* parameters show a small increase. This trend is in good agreement with previous works of Ni-substituted $GdBaCo_2O_{5+\delta}$ [19,24]. On the other hand, when $x > 0.4$, the lattice parameters show an inverse trend of evolution: the *b*-lattice parameter slightly decreases with increasing Ni, while the *a*-lattice parameter shows a small increase, meanwhile the *c* parameter remains approximately constant. Nevertheless, the cell volume shows an uneventful decrease with increasing Ni, highlighting the observation of the enhanced orthorhombic distortion along with Ni substitution.

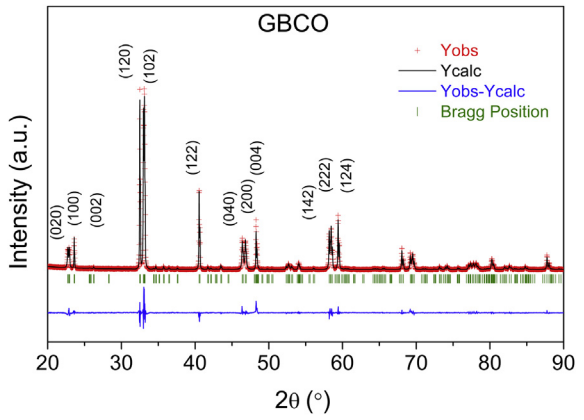

Fig. 2. Rietveld refinement for $GdBaCo_2O_{5+\delta}$ in the orthorhombic space group *Pmmm*; reliability factors are listed below. $R_{Bragg} = 4.83.4$; $R_F = 3.81$; $R_p = 12.2$; $R_{wp} = 15.3$; $R_{exp} = 9.43$, $\chi = 1.6$.

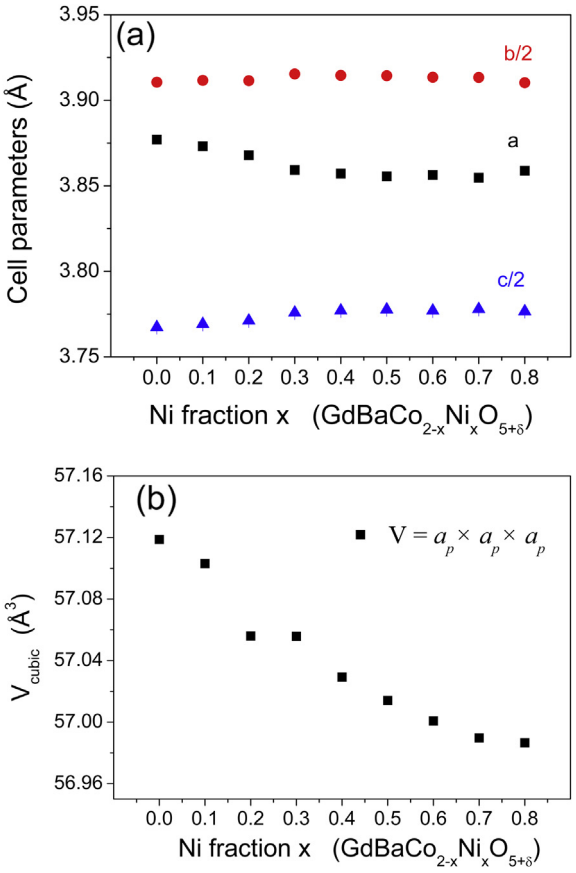

Fig. 3. Evolution of (a) cell parameters and (b) cubic unit cell volume with Ni substitution as obtained from Rietveld refinement.

3.2. Oxygen nonstoichiometry

The oxygen content of Ni-substituted compounds as determined by iodometric titration and thermogravimetry is listed in Table 1. For iodometry measurements, the δ value of each composition is averaged from three repeated titrations. The total oxygen constant remains roughly constant with the increase of Ni content and close to 5.5 when $x \leq 0.6$, suggesting that the average valence of both Co and Ni ions in those compositions is close to +3, which is in good accordance with the result of Bharathi et al. [24] in $GdBaCo_{2-x}Ni_xO_{5+\delta}$ as well as with the oxygen content of $GdBaCo_2O_{5+\delta}$ obtained from Conder et al. [22]. For $x = 0.7$ and $x = 0.8$, the decrease of oxygen content was more important but the compounds remain orthorhombic as mentioned above.

Fig. 4 shows examples of thermogravimetry reduction curves obtained in this work. The oxygen content analysis based on the

Table 1
Oxygen content of $GdBaCo_{2-x}Ni_xO_{5+\delta}$ obtained by iodometric titration and TG/H_2 and linear TEC as obtained from high-temperature XRD.

Ni content *x*	Oxygen content from iodometry	Oxygen content from TG/H_2	Thermal expansion (10^{-6} K^{-1})
0	5.51(2)	5.52	20.6
0.1	5.53(2)		
0.2	5.55(2)		
0.3	5.50(2)	5.51	19.8
0.4	5.53(2)		
0.5	5.50(2)		
0.6	5.50(2)	5.52	18.4
0.7	5.48(2)		
0.8	5.34(2)		

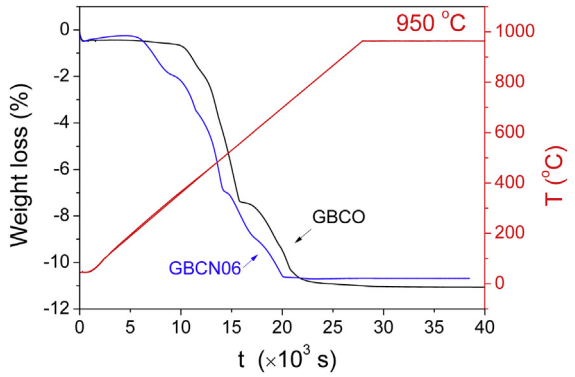

Fig. 4. TG curves of H_2 reduction for (a) GBCO and (b) GBCN06. Black line and red line represent the mass loss in percentage and temperature, respectively.

overall weight loss is related to a "final plateau" of the TG weight loss (in percentage) curve, which was considered as the accomplishment of reduction process, referring to a residual pure oxide mixture and metallic Co and Ni. The approximate starting temperature of the plateau is different for each composition. The final plateau can be obtained at nearly 800 °C for GBCO, which is in agreement with the previous work of Conder et al. [22], and at about 700 °C for Ni-substituted GBCN03 and GBCN06. The oxygen contents determined by TG/H_2 are slightly higher than those obtained by iodometry for pure GBCO and Ni-substituted GBCN03, GBCN06. Nevertheless, in general, these two methods seem in good accordance with each other, and the $GdBaCo_{2-x}Ni_xO_{5+\delta}$ compounds exhibit at room temperature an oxygen content close to 5.5, indicating an average valence of +3 for both Co and Ni cations up to $x = 0.7$.

3.3. Phase transitions

GBCO compound is known to present two-phase transitions between room temperature and 800 °C, which were studied in details earlier [10]. The low-temperature phase transition occurs at around 100 °C in GBCO [20] and has been also observed in analogous materials such as $TbBaCo_2O_{5+\delta}$ [27,28], $HoBaCo_2O_{5+\delta}$ [29,30] and $PrBaCo_2O_{5+\delta}$ [25,31]. This phase transition, associated to a metal-insulator transition, is attributed to a first-order LS to HS spin-state transition of the Co^{3+} ions located at the octahedral sites. The second transition occurs at high temperature, *i.e.* around 550 °C and is associated to the disordering of the oxygen sublattice. In this case, the structure changes from orthorhombic *Pmmm* to tetragonal *P4/mmm* space group. Here, the transitions have been explored by DSC and temperature-dependent XRD measurements.

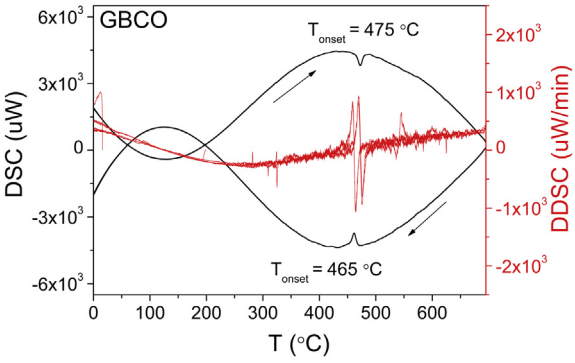

Fig. 5. Example of DSC curves for $GdBaCo_2O_{5+\delta}$: arrows indicate the heating and cooling runs, respectively. T_{onset} is the detected temperature where the phase transition takes place.

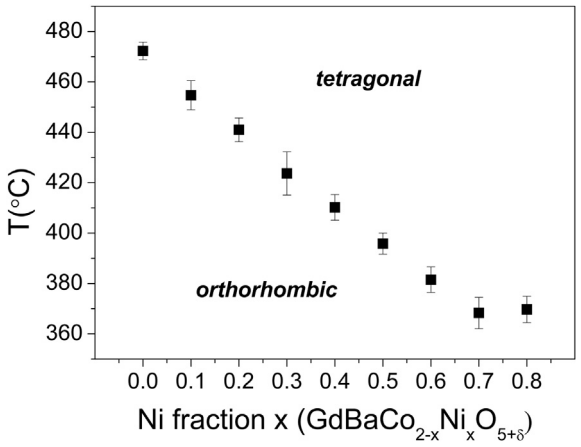

Fig. 6. Phase transition temperature for $GdBaCo_{2-x}M_xO_{5+\delta}$ (M = Ni, $x = 0.1, 0.2, \ldots$) as determined at high temperature from the T_{onset} on the heating DSC experiment.

The phase transitions have been firstly investigated by DSC, as shown in Fig. 5. Contrarily to previous studies [20], we were not able to detect the LT phase transition, probably due to different experimental conditions. This low-temperature transition was nevertheless detected through XRD as shown below. At elevated temperature, the small peaks on the DSC curve represent the onset of phase transitions, corresponding to the structural change from orthorhombic-to-tetragonal structural forms, with a hysteresis of about 10 °C between heating and cooling runs. The temperatures of HT phase transition determined by DSC in $GdBaCo_{2-x}Ni_xO_{5+\delta}$ ($x = 0.1$–0.8) are depicted in Fig. 6. Ni substitution reduces the temperature of the orthorhombic–tetragonal phase transition, reaching a limit for $x = 0.8$. This transition involves a rearrangement of oxygen vacancies from the low-temperature one-dimensional ordering along the *a* axis (orthorhombic) to the high-temperature two-dimensional random distribution essentially in Gd planes (tetragonal) [10].

The structural evolution as a function of temperature has been also investigated by high-temperature XRD. The acquisitions have been done every 25 or 50 °C in the low and high-temperature range, and every 10 °C close to expected phase transition temperatures. Fig. 7 presents the particular case of GBCO close to the high-temperature transition, evidenced by a vanishing of peaks indexed (040) and (200) in *Pmmm* symmetry and the successive appearance of a new peak indexed (004) in *P4/mmm* symmetry at this transition temperature. The corresponding thermal evolution of lattice parameters extracted by a Le Bail refinement is shown in Fig. 8. This

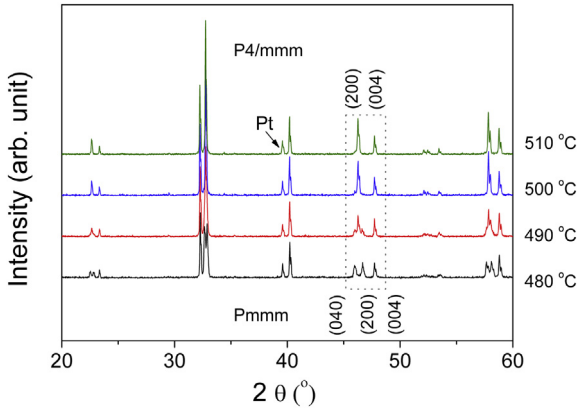

Fig. 7. Temperature-dependant XRD patterns of GBCO, at temperatures close to high-temperature phase transition.

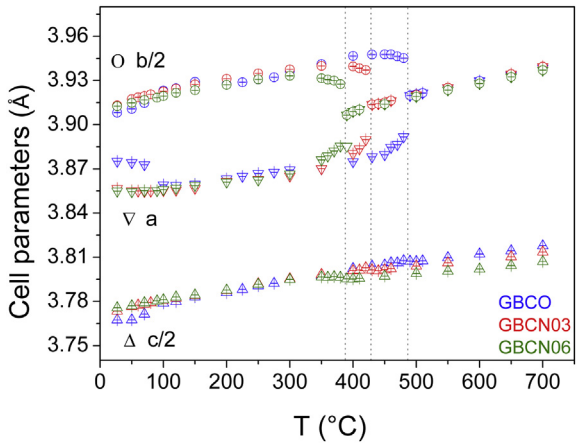

Fig. 8. Cell parameters of GBCO (blue), GBCN03 (red) and GBCN06 (green) as a function of temperature, as obtained from the Le bail fitting of temperature-dependent XRD data. (For interpretation of the references to colour in this figure legend, the reader is referred to the web version of this article.)

evolution clearly allows identifying the two transitions: a low-temperature (LT) structural transformation taking place at *ca.* 80 °C which corresponds to a sudden shrinking of *a*-lattice parameter and a lengthening of *b* and *c*; a high-temperature (HT) phase transition taking place at ca. 490 °C, in good agreement with previous work on GBCO [10]. This HT transition temperature also corresponds well to the DSC result of ca. 475 °C obtained in this work.

Ni-substituted GBCN03 and GBCN06 exhibit a similar phase transition from low-temperature orthorhombic *Pmmm* structure to high-temperature tetragonal *P4/mmm* structure, with a reduction of transition temperature with the increase of *x* in consistency with the results of DSC. The thermal evolution of the cell parameters and unit cell volume obtained by Le Bail refinement of high-temperature XRD data are shown in Figs. 8 and 9. Considering both DSC and XRD experiments, Ni substitution facilitates the occurrence of this HT phase transition by reducing the transition temperature, which could be attributed to an effect of disorder on cation sublattice and to a higher reducibility of the Ni-substituted compounds as shown by TG under hydrogen.

Similarly to the pristine GBCO, $GdBaCo_{2-x}Ni_xO_{5+\delta}$ ($x = 0.1$–0.8) compounds exhibit at room temperature an orthorhombic structure indexed in the *Pmmm* space group. In this case, the metal–insulator (MI) transition at low temperature, as represented by the sudden shrinking of lattice parameters mentioned above, is not observed. Recent studies in slightly Ni-substituted $LnBaCo_2O_{5+\delta}$ [24,32] revealed that Ni substitution could decrease the MI temperature as a consequence of the local structure distortions induced by Ni ions.

The unit cell volume increases nearly linearly with the temperature, even across the mentioned phase transitions. Therefore, the linear thermal expansion coefficient (α_L) can be derived from the volumetric thermal expansion coefficient, *i.e.* $\alpha_V \equiv 3\alpha_L$. The obtained linear thermal expansion coefficient (TEC) for $GdBaCo_2O_{5+\delta}$ is $20.6 \times 10^{-6}\ K^{-1}$ in the range of temperatures from 175 to 700 °C, in accordance with the TECs for cobaltites materials and reported TEC for GBCO [7,10,26]. The other linear thermal expansion coefficients (TEC) obtained from refined evolution of unit cell parameters are listed in Table 1. It is shown that the Ni substitution induces a slight decrease of α_L, and this trend is in agreement with the results from Bo Wei et al. [19] determined by dilatometry, despite a much smaller decrease is shown in our study. For example, for the Ni substitution $x = 0.3$, these authors obtained the TEC $= 15.5 \times 10^{-6}\ K^{-1}$ to be compared with the value TEC $= 19.8 \times 10^{-6}\ K^{-1}$ obtained in this work.

3.4. Electrical conductivity

The total electrical conductivities (σ) obtained under air using the AC four-point method are shown in Fig. 10, which reveals quite different temperature-dependent behaviors in the evolution of electrical conductivities between the pristine GBCO and the Ni-substituted GBCN03 and GBCN06.

The electrical conductivity behaviour of GBCO varies strongly over the investigated temperature range. Below 100 °C, GBCO exhibits a typical semiconductor-type behavior: starting from room temperature, the conductivity increases with increasing temperature by one order of magnitude, until a temperature close to 100 °C, above which the increase of σ becomes weaker. This corresponds to the metal–insulator (MI) transition resulting from the sudden spin-state switch for the Co^{3+} ions from LS to HS ($t_{2g}^4 e_g^2$) states at this temperature (T_{MI}). This is in good agreement with the low-temperature transition observed in the cell parameters evolution discussed above as well as in the literature [10,20,21]. Thereafter,

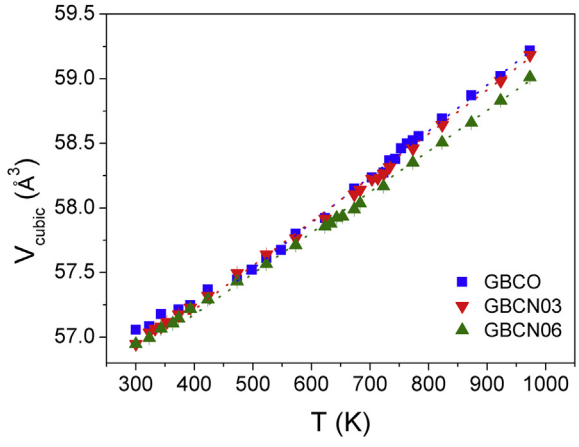

Fig. 9. Cubic unit cell volume evolution and fitting as a function of temperature of GBCO (blue), GBCN03 (red) and GBCN06 (green). (For interpretation of the references to colour in this figure legend, the reader is referred to the web version of this article.)

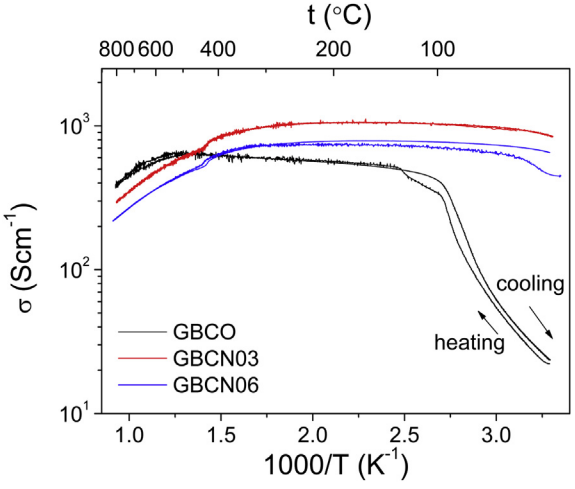

Fig. 10. Electrical conductivity as a function of temperature measured with rectangular bar sample by AC four-points method.

the conductivity of GBCO gradually increases with the increasing temperature, showing still semiconductor-type behavior although with very weak temperature dependence, and then passes through a maximum value in σ in the temperature range 500–600 °C, from which the electrical conductivity decreases with increasing temperature indicating a metallic-like behavior, in accordance with references [5–7,10,33]. The evolution of conduction properties at high and intermediate temperature is linked first with the evolution of oxygen content with temperature, affecting directly the concentration of charge carriers. On the other side, the alternation of CoO_5 pyramidal and CoO_6 octahedral planes along the *b* direction in the orthorhombic phase certainly affects the hole mobility by changing Co-O distances and thus orbitals overlapping. From this, it is difficult to give a precise explanation of the evolution of conductivity in the intermediate temperature range (100–500 °C). We can nevertheless estimate that the very small evolution of conductivity is due to a subtle balance between the thermally activated mobility of holes and the diminishing of hole concentration due to oxygen loss. At high temperature, *i.e.* slightly above the high-temperature transition, the concentration of electrons becomes higher than that of holes [34]. Nevertheless, since holes have a 7–8 times higher mobility than electrons [35], the conductivity is still essentially controlled by holes at high temperature, till ~800 °C. The metallic behavior, *i.e.* the diminishing of conductivity with temperature is due to the fact that hole concentration diminishes faster than mobility increase, this last being thermally activated.

The behavior of GBCN03 and GBCN06 compounds at high temperature is very similar to that of pure GBCO; one thus may expect the same behavior to be observed, *i.e.* the diminishing of holes concentration at high temperature becomes faster than the increase of hole mobility. The low-temperature behavior is in the case of Ni-doped GBCO different from that of pure GBCO. The MI transition is no longer visible in the evolution of σ, in agreement with the results of XRD showing no shrinking of cell parameters for GBCN03 and GBCN06 between RT and 100 °C. Therefore, we can assume that the T_{MIT} has been reduced by the Ni substitution till a temperature below our investigated range. This probably results from the decrease of energy necessary for spin-state transition (MI) due to the structural distortion and crystal field energies modification with Ni substitution, which is consistent with previous work of Bharathi et al. [24].

At high temperatures corresponding to the operating temperature range for IT-SOFC, the electrical conductivity has been slightly reduced by increasing Ni substitution, giving rise to the lowest value for GBCN06. Nevertheless, all these materials have shown adequate electrical conductivities (>100 S cm^{-1}), which ensures their potentials as cathodes for IT-SOFC application.

3.5. Electrochemical characterization

Fig. 11 shows the temperature-dependent impedance spectra of (50 wt.% GBCN03 – 50 wt.% CGO)/CGO/(50 wt.% GBCN03 – 50 wt.% CGO) symmetric cells and their corresponding equivalent circuits. Over the investigated temperatures, the polarization resistances can be generally separated into two contributions, represented by two partially overlapped depressed semi-circles as observed in the Nyquist plots: a high frequency contribution (R1) attributed to the electronic and ionic charge-transfer processes and a low frequency contribution (R2) related to the complex non-charge-transfer processes in oxygen reduction mechanism, respectively. It is apparent that the contribution at low frequency range (R2), which is the smaller part at higher temperatures, increase more significantly than the high frequency with decreasing temperature and finally becomes predominant at lower temperatures.

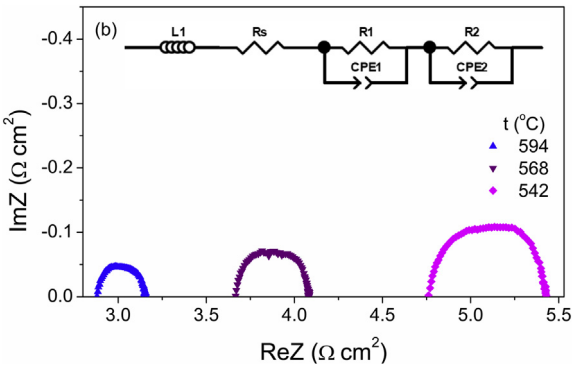

Fig. 11. Nyquist plots of impedance spectra of (50 wt.% GBCN03 – 50 wt.% CGO)/CGO/(50 wt.% GBCN03 – 50 wt.% CGO) symmetric cell and their corresponding equivalent circuits (see text for details).

Fig. 12 shows the Arrhenius plots of the obtained electrolyte conductivity and the electrode ASR. Whatever the composition of composite electrode is, the obtained electrolyte conductivities exhibit very close values and identical temperature-dependent behavior with the same activation energy value (E_a = 0.69 eV), in consistency with the widely known performance of CGO. Thus, the

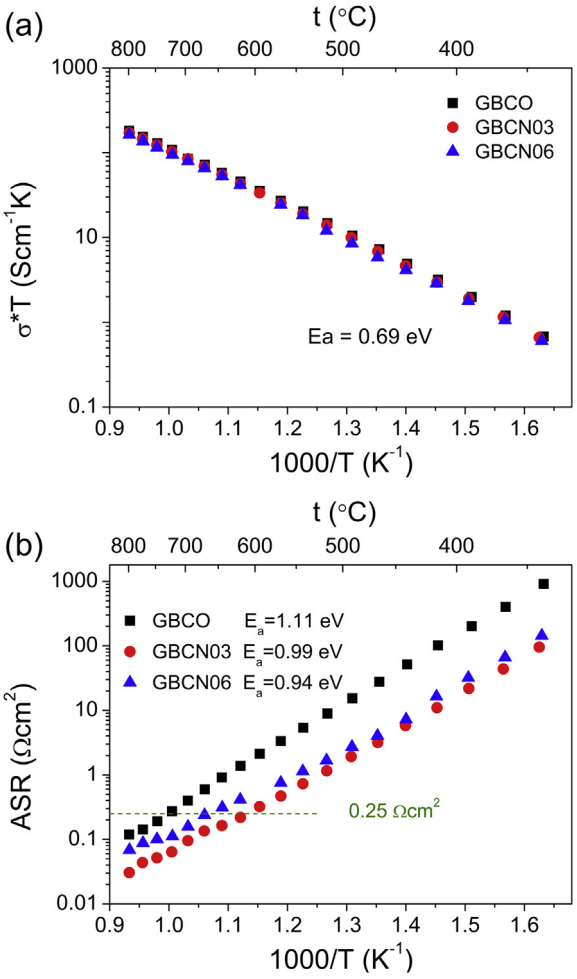

Fig. 12. Arrhenius plots of (a) the conductivity of CGO electrolytes with different electrode materials and (b) the electrode polarization resistances, obtained from the impedance spectra on the (50 wt.% $GdBaCo_{2-x}Ni_xO_{5+\delta}$ – 50 wt.% CGO)/CGO/(50 wt.% $GdBaCo_{2-x}Ni_xO_{5+\delta}$ – 50 wt.% CGO) symmetric cells.

absence of extended detachment at electrode/electrolyte interface and a good interfacial adhesion could be certified. On the other hand, the composite cathodes demonstrate slightly different electrochemical properties. The GBCO composite cathode shows the highest ASR values over the investigated temperature range, whilst smaller ASR have been obtained for the GBCN03 and GBCN06, even though the origin of the effect of Ni substitution in the cathode materials remains still ambiguous. However, the calculated activation energy has been reduced from 1.11 eV to 0.94 eV with increasing Ni substitution. The acknowledged standard value for cathode materials, ASR = 0.25 Ω cm^2 could be obtained approximately at 726 °C, 610 °C and 670 °C for the GBCO, GBCN03 and GBCN06 composite cathodes, respectively, revealing attractive electrochemical performances in the temperature range of interest and indicating their potentials as cathode materials for IT-SOFC application.

4. Conclusion

In this work, wet chemical routes haven been applied to synthesize the $GdBaCo_{2-x}Ni_xO_{5+\delta}$ (x = 0, 0.1, 0.2, …) and allowed to obtain a high level of substitution with a solubility up to $x = 0.8$. Ni substitution is shown to sustain the orthorhombic structure and to enhance the orthorhombic distortion. Oxygen contents for the materials at room temperature have been determined by iodometry and thermogravimetry showing no distinct variation of oxygen stoichiometry with Ni substitution. The phase transition at elevated temperature has been investigated by DSC and XRPD and is shown to occur at lower temperature as Ni content increases.

Three compositions with $x = 0$, 0.3 and 0.6 have been chosen for further structural, electrical and electrochemical characterization. Both the obtained temperature-dependent evolution of cell parameters and the electrical conductivity suggest that two type of transitions: low-temperature MI transition and the high-temperature phase transition, have been facilitated by the Ni substitution. High-temperature XRD reveals that the Ni substitution can slightly help to decrease the TEC of the pristine GBCO. However, the obtained TECs are still close to 20 × 10^{-6} K^{-1} and thus still high if compared to those of standard electrolyte materials. The electrical conductivities as measured by AC four-point method are in the expected range for electrode materials for all compositions. The electrochemical characterization has been performed on symmetric cells by using composite electrode to avoid extended delamination due to expansion mismatch. All compounds show excellent electrochemical properties; the best results are obtained for $x = 0.3$, GBNC03 showing a very low polarization resistance as low as 0.25 Ω cm^2 at 625 °C.

Acknowledgement

This work has been supported by the French Agence Nationale de la Recherche (ANR) through the project NanOxyDesign.

References

[1] A.A. Taskin, A.N. Lavrov, Y. Ando, Physical Reviews B 71 (2005) 28.
[2] A.A. Taskin, A.N. Lavrov, Y. Ando, Applied Physics Letters 86 (2005) 3.
[3] A.A. Taskin, A.N. Lavrov, Y. Ando, Progress in Solid State Chemistry 35 (2007) 481–490.
[4] A. Tarancon, S.J. Skinner, R.J. Chater, F. Hernandez-Ramirez, J.A. Kilner, Journal of Materials Chemistry 17 (2007) 3175–3181.
[5] J. Pena-Martinez, A. Tarancon, D. Marrero-Lopez, J.C. Ruiz-Morales, P. Nunez, Fuel Cells 8 (2008) 351–359.
[6] M.B. Choi, S.Y. Jeon, J.S. Lee, H.J. Hwang, S.J. Song, Journal of Power Sources 195 (2010) 1059–1064.
[7] N. Li, Z. Lu, B.O. Wei, X.Q. Huang, K.F. Chen, Y.Z. Zhang, W.H. Su, Journal of Alloys and Compounds 454 (2008) 274–279.
[8] Y. Lee, D.Y. Kim, G.M. Choi, Solid State Ionics 192 (2011) 527–530.
[9] Y.K. Tang, C.C. Almasan, Physical Reviews B 77 (2008) 5.
[10] A. Tarancon, D. Marrero-Lopez, J. Pena-Martinez, J.C. Ruiz-Morales, P. Nunez, Solid State Ionics 179 (2008) 611–618.
[11] L.W. Tai, M.M. Nasrallah, H.U. Anderson, D.M. Sparlin, S.R. Sehlin, Solid State Ionics 76 (1995) 259–271.
[12] H. Lv, Y.-J. Wu, B. Huang, B.-Y. Zhao, K.-A. Hu, Solid State Ionics 177 (2006) 901–906.
[13] P. Hjalmarsson, M. Søaard, M. Mogensen, Solid State Ionics 180 (2009) 1290–1297.
[14] H. Nagamoto, I. Mochida, K. Kagotani, H. Inoue, A. Negishi, Journal of Materials Research 8 (1993) 3158–3162.
[15] N. Ortiz-Vitoriano, I.R. de Larramendi, J.I.R. de Larramendi, M.I. Arriortua, T. Rojo, Journal of Power Sources 192 (2009) 63–69.
[16] R. Chiba, F. Yoshimura, Y. Sakurai, Solid State Ionics 124 (1999) 281–288.
[17] H. Ding, X. Xue, International Journal of Hydrogen Energy 35 (2010) 4316–4319.
[18] Y.N. Kim, J.H. Kim, A. Manthiram, Journal of Power Sources 195 (2010) 6411–6419.
[19] B. Wei, Z. Lü, D. Jia, X. Huang, Y. Zhang, W. Su, International Journal of Hydrogen Energy I35 (2010) 3775–3782.
[20] C. Frontera, J.L. García-Muñoz, A. Llobet, M.A.G. Aranda, Physical Reviews B 65 (2002) 180405.
[21] A. Maignan, C. Martin, D. Pelloquin, N. Nguyen, B. Raveau, Journal of Solid State Chemistry 142 (1999) 247–260.
[22] K. Conder, E. Pomjakushina, A. Soldatov, E. Mitberg, Materials Research Bulletin 40 (2005) 257–263.
[23] M. Karppinen, M. Matvejeff, K. Salomäki, H. Yamauchi, Journal of Materials Chemistry 12 (2002) 1761–1764.
[24] A. Bharathi, P. Yasodha, N. Gayathri, A.T. Satya, R. Nagendran, N. Thirumurugan, C.S. Sundar, Y. Hariharan, Physical Reviews B 77 (2008) 8.
[25] C. Frontera, J.L. García-Muñoz, A.E. Carrillo, C. Ritter, D. Martín y Marero, A. Caneiro, Physical Reviews B 70 (2004) 184428.
[26] E.V. Tsipis, V.V. Kharton, Journal of Solid State Electrochemistry 12 (2008) 1039–1060.
[27] Y. Moritomo, T. Akimoto, M. Takeo, A. Machida, E. Nishibori, M. Takata, M. Sakata, K. Ohoyama, A. Nakamura, Physical Reviews B 61 (2000) R13325.
[28] I. Troyanchuk, A. Chobot, D. Khalyavin, R. Szymczak, H. Szymczak, Journal of Experimental and Theoretical Physics 95 (2002) 748–752.
[29] F. Fauth, E. Suard, V. Caignaert, B. Domengès, I. Mirebeau, L. Keller, European Physics Journal, B 21 (2001) 163–174.
[30] L. Malavasi, M. Brunelli, Y. Diaz-Fernandez, B. Pahari, P. Mustarelli, Physical Reviews B 80 (2009) 153102.
[31] S. Streule, A. Podlesnyak, E. Pomjakushina, K. Conder, D. Sheptyakov, M. Medarde, J. Mesot, in: International Conference on Strongly Correlated Electron Systems (SECES 05), Elsevier Science Bv, Vienna, Austria, 2005, pp. 539–540.
[32] B. Raveau, C. Simon, V. Caignaert, V. Pralong, F. Lefevre, Journal of Physics: Condensed Matter 18 (2006) 10,237.
[33] K. Zhang, L. Ge, R. Ran, Z. Shao, S. Liu, Acta Materialia 56 (2008) 4876–4889.
[34] D.S. Tsvetkov, V.V. Sereda, A.Yu. Zuev, Solid State Ionics 180 (2010) 1620–1625.
[35] D.S. Tsvetkov, V.V. Sereda, A.Yu. Zuev, Solid State Ionics 192 (2011) 215–219.